LOW FREQUENCY DIELECTRIC PROPERTIES OF THREE BENTONITES AT DIFFERENT ADSORBED WATER STATES

Heike Kaden[a,b], Franz Königer[a,b], Maria Strømme[c], Gunnar A. Niklasson[c]; Katja Emmerich[a]

[a] Competence Center for Material Moisture, Karlsruhe Institute of Technology, Karlsruhe, Germany,
[b] Institute of Functional Interfaces at Karlsruhe Institute of Technology (KIT), Karlsruhe, Germany
[c] Department of Engineering Sciences, The Ångström Laboratory, Uppsala University, Uppsala, Sweden

Heike Kaden (corresponding author)
heike.kaden@kit.edu
+49 721 608 2 6114
Herrman-von-Helmholtz-Platz 1
76344 Eggenstein-Leopoldshafen
Germany

Franz Königer
franz.koeniger@kit.edu
Herrman-von-Helmholtz-Platz 1
76344 Eggenstein-Leopoldshafen
Germany

Maria Strømme
Maria.Stromme@angstrom.uu.se
Box 534
75121 Uppsala
Sweden

Gunnar A. Niklasson
Gunnar.niklasson@angstrom.uu.se
Box 534
75121 Uppsala
Sweden

Katja Emmerich
Katja.emmerich@kit.edu
Herrman-von-Helmholtz-Platz 1
76344 Eggenstein-Leopoldshafen
Germany

LOW FREQUENCY DIELECTRIC PROPERTIES OF THREE BENTONITES AT DIFFERENT ADSORBED WATER STATES

Heike Kaden[a,b], Franz Königer[a,b], Maria Strømme[c], Gunnar A. Niklasson[c], Katja Emmerich[a]

[a] Competence Center for Material Moisture, Karlsruhe Institute of Technology, Karlsruhe, Germany
[b] Institute of Functional Interfaces at Karlsruhe Institute of Technology (KIT), Karlsruhe, Germany
[c] Department of Engineering Sciences, The Ångström Laboratory, Uppsala University, Uppsala, Sweden

KEYWORDS: clay mineral, layer silicate, smectite, bound water, permittivity, equivalent circuit

ABSTRACT

Three bentonites of varying smectite content were investigated by dielectric spectroscopy in the frequency range 10^{-4} to 10^{6} Hz after storage at well-defined humidities. The identification of relaxation processes from complex permittivity measurements was difficult, since conductivity effects were superimposed on the underlying relaxations. Relaxation peaks revealed by the dissipation factor indicated the occurrence of interfacial processes between 10^{2} and 10^{6} Hz. The intensity of the polarization of the electrochemical double-layer at the clay-water interface was promoted by increasing water content and was shifted to higher frequencies the higher the water content in the bentonites. Below ~ 1 Hz electrode polarization (EP) was shown to be a participating process with capacitance values ranging from $0.6*10^{-3}$ to $7.3*10^{-3}$ F due to the accumulated charges. An equivalent circuit model was introduced that successfully described the low frequency dielectric behaviour of bentonites at low moisture levels. An included series R-CPE connection was used to describe the double-layer relaxation. At water contents up to 17% the bulk resistivity was mainly influenced by smectite content and cation exchange capacity, whereas at water contents of ≥ 19% interlayer occupation and hydration state became more important.

INTRODUCTION

Bentonites are natural materials occurring on surface and subsurface deposits around the world [1]. They consist of major amounts of the swellable clay mineral montmorillonite or other minerals of the smectite group. Since even the swellable 2:1 layer silicate montmorillonite widely varies in composition and structure [2], a detailed knowledge about their mineralogical features is substantial to understand the influence on the macroscopic behaviour of the bentonites [3-5].

Due to specific properties of smectites, for instance high sorption capacity and their ability to reversibly exchange cations, smectite-rich materials, such as bentonites, are widely used for industrial and environmental applications. They have gained an increasing importance in the field of waste disposal of hazardous materials, like radioactive substances, but are also – along with other clays – used as fillers and major components in cosmetics and pharmaceuticals [6, 7]. In agriculture, high clay content together with the presence of 2:1 clay minerals is associated with high soil fertility. Processes due to clay mineral intrinsic properties, such as water retention and provision of exchangeable sites for the essential nutrients in plant growth, are predominant features increasing soil fertility [1].

For many environmental and industrial applications it is crucial to accurately adjust the water content of the mineral mixtures. Hence, the precise determination of water content is necessary for instance to ensure high quality products and to assess the stability of the geotechnical barriers on waste disposal sites. However, the water binding mechanisms are complex in clay minerals [8-11]. Swellable clay minerals bind water on their outer and on their inner surface upon hydration, whereas the interlayer cations undergo stepwise hydration, which is influenced by valence and radii of the cations [12]. With increasing relative humidity an increasing amount of water molecules is associated to the interlayer cations that can be described by different hydration states ranging from 0W to 3W [13].

Several techniques were established for the determination of water content [14], among which static heating at 105 °C until weight equilibrium is commonly used and regularly applied as a reference method [15]. Beside heating, indirect physical methods like tensiometric techniques,

geophysical methods (e.g. electrical conductivity technique), nuclear approaches (e.g. neutron-scattering technique) as well as several high frequency electrical techniques [16] and remote sensing techniques [17] are in use [18, 19]. Each technique is characterized by individual features, such as accuracy, spatial resolution, time consumption and cost, and further holds different requirements on sample amount and preparation. The preciseness of the different water content measurement approaches may vary distinctively, especially when determining the water content of materials containing substantial amounts of swellable clay minerals. In many applications, such as the assessment of geotechnical barriers in landfill sites, in-situ and non-destructive water content determination is required.

Thus, moisture measurement by means of dielectric spectroscopy, which uses the relationship between the real relative permittivity and the volumetric water content of a sample, is a promising technique, and it has been shown that both the state of water (bound or free) [20] as well as the number of dissociated water molecules carrying charges in a system [21-23] can be studied with this technique. Moreover, it is not restricted by safety regulations in contrast to nuclear approaches [19, 24]. However, recent work shows that the regularly used frequency of about 1 GHz seems to be unsuitable for water content determination with dielectric spectroscopy when the studied materials contain a major amount of swellable clay minerals [25].

A wide range of studies was carried out regarding the determination of volumetric water content of soils by dielectric spectroscopy [26-30] and they showed that a number of parameters, such as bulk density [31] and iron content [32] influences the results in laboratory and in the field. Moreover, swelling clays [33, 34] as well as non-swelling clays [35] were investigated by dielectric spectroscopy over a wide moisture range to study the clay specific behaviour such as flocculation and gel formation and the role of cations as mobile charge carriers.

Most of the dielectric studies performed on clays were conducted at high moisture levels, on suspensions or pastes [36-41]. However, in many of the industrial and environmental

applications where the moisture is required to be monitored, such as for sealing layers in hazardous waste disposal sites, clays are present at much lower water contents.

Our own investigations on swellable and non-swellable 2:1 layer silicates showed a higher sensitivity of low-frequency measurements (10^{-4} ... 10^{6} Hz) compared to high-frequency measurements ($2.0*10^{8}$... $1.1*10^{9}$ Hz) to display differences in the adsorbed water state [25]. Still, low frequency dielectric analysis of clay-water-systems has commonly been conducted on clay suspensions or clay-water-electrolyte systems [34, 40-42]. In contrast to mid and high frequency measurements, within the low-frequency range further polarization mechanisms, e.g. interfacial polarization, double-layer polarization and electrode polarization, may influence the dielectric spectra and superimpose on the bound water effect. A four terminal probe was suggested by Carrier and Soga [43] as a preliminary method to reduce electrode polarization effects within the low frequency range. Furthermore, some experimental and mathematical approaches were established to correct dielectric data for the contribution of electrode polarization [44-47].

Previous equivalent circuit fitting of clay-water-systems similarly concentrated on clay suspensions [40, 42, 48]. Dielectric studies on clays at low water content states and their assessment by equivalent circuit fitting is rarely described in the literature.

The aim of the current study is to investigate the dielectric behaviour of three bentonites with varying smectite content within the low-frequency range. The materials are studied at different adsorbed water states rather than as clay suspensions or clay pastes. Additionally, equivalent circuit fitting was implemented in order to evaluate the influence of the attributing polarization mechanisms as a function of varying humidity.

MATERIALS

Dielectric properties of three bentonites were studied at different hydration states in the low-frequency range. The bentonite “Volclay” (ben_Vol), “Calcigel” (ben_Cal) and bentonite “P” (ben_P) were provided by Süd-Chemie AG, Germany. Basic physical and mineralogical properties, such as mineralogical composition, cation exchange capacity (CEC), type of

exchangeable cations, grain size distribution as well as surface properties such as outer specific surface area ($A_{s, out}$), total specific surface area ($A_{s, total}$), and pore size distribution were determined. Hereby, the mineralogical composition was determined by means of X-ray diffraction analysis and the grain size distribution by sieving and sedimentation analysis. The CEC was determined photometrically according to the Cu(II)-Triethylenetetramine method [49] and the type of exchangeable cation of the supernatant from the copper-complex exchange reaction by inductively coupled plasma - optical emission spectroscopy (ICP-OES). Surface properties were investigated by nitrogen and water vapour adsorption isotherms, whereas the specific surface area were determined according to Brunauer-Emmett-Teller theory [50] and the pore size distribution according to the non-local density functional theory [51] using the adsorption branch model for cylindrical silica pores. A detailed description of the related experiments can be found in [52].

The fine grained powders were stored under defined relative humidity (r.h.) conditions and prevented from previous heating or drying before the hydration experiments.

Among the studied bentonites, the ben_P exhibits the lowest amount of impurities, consisting of about 98% of swellable minerals belonging to the smectite group (Table 1). Ben_Vol is characterized by the second highest smectite content being about 78%. The material furthermore contains about 10% feldspars, 8% mica/illite, 4% quartz and traces of gypsum. The third material, ben_Cal, exhibits the smallest smectite content (about 65%) and the highest amount of impurities. Major phases beside the smectites are non-swellable 2:1 layer silicates, such as mica/illite (17%) and 7% of quartz. The clay content of the materials, i.e. the fraction of < 2µm, decreases in the order ben_P > ben_Vol > ben_Cal (Table 1).

The different mineralogical composition and particle size distribution of the bentonites is further displayed by varying exchange and surface properties. The CEC for instance is connected to the amount of swellable phases and their layer charge. The ben_P exhibits the highest CEC (119 meq/100g) due to its high smectite content and the high layer charge of the smectite. The ben_Vol exhibits an intermediate CEC (83 meq/100g) and the ben_Cal the lowest CEC of the three bentonites (63 meq/100g). Since the bentonites are natural bulk

materials their interlayer occupation is heterogeneous (Table 1). The interlayer of the smectite in ben_P is equally occupied by monovalent (51%) and divalent cations (49%), whereas the ben_Vol is slightly dominated by monovalent cations (64%) and the ben_Cal is clearly dominated by divalent cations (89%).

The external surface area ($A_{s,\ out}$) is primarily influenced by grain size and porosity of a material. Since ben_P displays the highest clay content (79%) of the three bentonites, a high $A_{s,\ out}$ of 105 m^2/g is in agreement with the grain size distribution. However, ben_Vol with a similarly high clay content exhibits a distinctively smaller $A_{s,\ out}$ of about 33 m^2/g, whereas ben_Cal, which is the coarsest of the materials with a silt content of about 50%, exhibits a distinctively higher $A_{s,\ out}$ of about 72 m^2/g. Accordingly, nitrogen adsorption experiments and analysis by means of non-local density functional theory revealed that ben_Cal is characterized by higher cumulated surface area of the pores than ben_Vol (Table 1).

The total specific surface area ($A_{s,\ total}$), which characterizes the sum of the external surface area as well as the interlayer surface, is strongly influenced by the hydration properties of the material, such as accessibility of the interlayer displayed by CEC as well as the type of interlayer cation. Consequently, the $A_{s,\ total}$ decreases with decreasing CEC in the order ben_P > ben_Vol > ben_Cal.

Table 1: Basic physical and mineralogical properties including mineralogical composition, type of interlayer cation, outer specific surface area ($A_{s,\ out}$) and total specific surface area ($A_{s,\ total}$) as well as cumulative surface area of micropores ($A_{s,\ micro}$) and mesopores ($A_{s,\ meso}$).

		Unit	Ben_Cal	Ben_Vol	Ben_P
Particle density		[g/cm³]	2.66	2.69	2.65
CEC		[meq/100g]	63	83	119
Exchangeable cations	Na	[%]	9	62	50
	K		2	2	1
	Ca		62	30	40
	Mg		27	6	9
Grain size	Sand	[wt%]	3	3	0
	Silt		50	20	21
	Clay		47	77	79
$A_{s,\ out}$		[m²/g]	72	33	105
$A_{s,\ total}$			289	378	417
$A_{s,\ micro}$	d < 2 nm		49	19	75
$A_{s,\ meso}$	d < 50 nm		78	35	117
Mineral	Calcite	[%]	3	-	-
	Dolomite		5	-	-
	Gypsum		-	< 1	-
	Kaolinite		3	-	-
	Mica/Illite		17	8	1
	K-Feldspars		-	6	-
	Plagioclases		-	4	-
	Quartz		7	4	1
	Dioctahedral smectite		65	78	98

METHODS

Pre-treatment

The powdered materials as received were stored in desiccators above saturated salt solutions until equilibration to specific r.h.. The salt solutions used for humidity equilibration were LiCl for 11% r.h., K_2CO_3 for 43% r.h. and KNO_3 for 93% r.h..

Determination of hydration state

The main hydration state of the smectites was evaluated by determining the predominant number of hydration shells around the interlayer cations. Since the position of the d*001* basal reflections of the smectites is a function of the extent of interlayer cation hydration, the

stepwise expansion of the smectites upon hydration, which is caused by intercalation of 0, 1, 2 or 3 planes of water within the interlayer, can be determined from the shift of the d*001* with varying water content of the sample [53]. Hereby, powder X-ray diffraction (XRD) specimen of the equilibrated samples were prepared and measured using a diffractometer with monochromator, apertures of 1 mm and 0.1 mm, and CuKα radiation in a range of 5 to 35° 2θ with a step size of 0.03° 2θ/3 s (D5000 diffractometer, Siemens, Germany) and the position of the d*001* was determined. Different hydration states are characterized for smectites as shown in Table 2.

Table 2: Hydration states of smectites, according to Ferrage *et al.* [53].

Hydration state	Abbreviation	d*001* [Å]
Dehydrated	0W	9.7 … 10.2
Monohydrated	1W	11.6 … 12.9
Bihydrated	2W	14.9 … 15.7
Trihydrated	3W	18 … 19

However, even under controlled conditions different hydration states coexist and are common in smectites [53]. Hence, transition states, such as 0W/1W, 1W/2W and 2W/3W, and even the coexistence of three hydration states are possible. Furthermore part of the interlayer water is connected to interlayer cations and part is connected to the interlayer clay mineral surface[54]. The water binding mechanisms on clay minerals are complex. Nevertheless, the increase of the d*001* is useful to display the expansion of the interlayer due to water uptake between the clay sheets. In the following, the d*001* will be used to demonstrate the swelling of the interlayer caused by the gradual water uptake for reasons of simplifying this complex topic.

Determination of water content

The moisture of the samples was determined by static and dynamic heating. Static heating was performed in duplicate by heating about 500 mg of the sample in glasses for 24 h at 105 °C and determining the weight loss caused by heating [55]. Hereby, the geotechnical

water content (W_{gt}) was determined (eq. (1)). W_{gt} refers to the dry weight of the sample as the reference base and is calculated as the ratio of mass of water (m_w) to dry weight (m_d) of the sample.

$$W_{gt}[\%] = \frac{m_w}{m_d} \cdot 100 \quad (1)$$

Dynamic heating was realized with Simultaneous Thermal Analysis (STA), where the thermal properties were determined in a defined temperature-time-program with the device STA 449 C Jupiter (Netzsch, Germany) and the experimental parameters listed in Table 3.

Table 3: Experimental parameters for STA measurements.

Parameter	Agent	Amount	Unit
crucible	Pt/Rh, with lid		
reference	empty Pt/Rh crucible with lid		
purging gas	synthetic air	50	ml/min
protective gas	nitrogen, quality 6.0 (99.999%)	20	ml/min
start temperature	-	35	°C
final temperature	-	1100	°C
heating rate	-	10	K/min
net weight	sample	100	mg

The mass loss of the dehydration was determined from the Thermogravimetry curve (TG) and was used to determine W_{gt}. With help of Differential Scanning Calorimetry (DSC) and the water release observed from Evolved Gas Analysis (EGA) with a coupled mass spectrometer, a material-specific temperature range of dehydration was determined, which was in the range of 35 – 250 °C for ben_Cal and ben_P, and 35 – 200 °C for ben_Vol.

Dielectric measurements

The dielectric properties were studied with the ALPHA-AN-Analyzer (Novocontrol) and the software WinDETA 5.0 within a frequency range of 10^{-4} to 10^{6} Hz and a fixed voltage of

220 1.5 V. After a small sample amount of about 500 mg was mounted between the two
221 electrode plates made of stainless steel, the plates were adjusted with a micrometer screw
222 and the thickness noted. The upper electrode incorporated a guard ring in order to eliminate
223 edge and surface current effects, such as stray capacitance at the electrode edges as well
224 as leakage current flows on the sample surface. The upper signal electrode had a diameter
225 of 10 mm and the lower electrode a diameter of 30 mm. Thus, the effective sample volume
226 was determined by the upper signal electrode incorporating the guard ring (Figure 1). After
227 mounting the sample, the sample cell was transferred into a stainless steel container, which
228 was prepared with the same salt solution that was used for moisture pre-equilibration of the
229 material. Thereafter, the container was sealed with Parafilm® (Merck) for the duration of the
230 measurement to avoid humidity influences from the environment. The sample cell used is
231 described in further detail elsewhere [56].
232

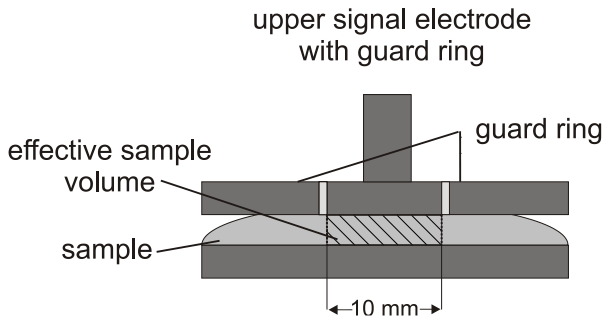

Figure 1: Schematic set up of the electrode plates with mounted sample.

233 For each of the bentonites, complex permittivity, complex resistivity and complex electrical
234 conductivity were determined. The relationship between these parameters is shown in eq.
235 (2), (7) and (5) below. The complex dielectric permittivity (ε^*) depends on angular frequency
236 ($\omega = 2\pi f$) and can directly be calculated from the complex capacitance C^*.

$$\varepsilon^*(\omega) = \frac{C^*(\omega)}{C_0}, \tag{2}$$

237 where $C_0=\varepsilon_{air}A/d$ is the capacitance of the empty cell, A is the electrode area and d is sample
238 thickness. The real part of the dielectric permittivity is denoted by ε' and the imaginary part

by ε''. The imaginary part of permittivity characterizes the dielectric loss of a medium and comprises contributions from relaxation processes (ε''_{relax}) and from the dc conductivity (σ_{dc}):

$$\varepsilon^* = \varepsilon' - i\left(\varepsilon''_{relax} + \frac{\sigma_{dc}}{\omega\varepsilon_0}\right) \quad (3)$$

where ε_0 describes the permittivity of vacuum being ~8.85*10^{-12} F/m.

The dissipation factor ($\tan\delta$), which can be used to identify relaxation processes, is given by eq. (4):

$$\tan\delta = \frac{\varepsilon''}{\varepsilon'} \quad (4)$$

The complex conductivity σ^* is related to the complex permittivity as

$$\sigma^* = i\omega\varepsilon_0\varepsilon^*, \quad (5)$$

and it comprises a real (σ') and an imaginary part (σ''):

$$\sigma^*(\omega) = \sigma'(\omega) + i\sigma''(\omega) \quad (6)$$

Further, the relation between the complex resistivity and the complex conductivity is expressed as

$$\rho^*(\omega) = \frac{1}{\sigma^*(\omega)}. \quad (7)$$

Equivalent circuit modelling

Equivalent circuit modelling was implemented using the software ZView (version 3.2c, Scribner Associates) in order to be able to describe the response of the bulk system by idealized model circuits. The quality of the fit describing the match of the sample impedance with that of the modelled impedance of the equivalent circuit is described by the weighted sum of squares (χ^2).

RESULTS AND DISCUSSION

Moisture / adsorbed water states

The hydration of the bentonites with increasing r.h. could clearly be observed from gravimetric water contents determined by static and dynamic heating (Table 4). The maximum amount of adsorbed water at 93% r.h. increased with increasing smectite content and increasing CEC (ben_P > ben_Vol > ben_Cal). However, this dependency was different for the samples stored at 11% and 43% r.h.. For these lower relative humidities the amount of adsorbed water sorted in the order ben_P > ben_Cal > ben_Vol. This order equals the order of the $A_{s,\,out}$. Hence, the water adsorption at low and intermediate r.h. was influenced by multiple factors, such as porosity of the sample, CEC and type of interlayer cation with the specific hydration energy, whereas the water adsorption at high r.h. was mainly influenced by the CEC and $A_{s,\,total}$, i.e. the water adsorption at the inner surface for instance by hydration of interlayer cations.

Table 4: Gravimetric water content determined by static and dynamic heating as well as hydration state of the smectites of the three bentonites stored at different relative humidities.

Sample	Parameter	Upper temperature		Humidity [%] 11	43	93
ben_Cal	static heating	105 °C	W_{gt} [%]	7.3	9.4	18.5
	dynamic heating	250 °C		10.3	12.7	18.9
	hydration state	-	-	1W/2W	1W/2W	2W/3W
ben_Vol	static heating	105 °C	W_{gt} [%]	4.4	7.3	19.6
	dynamic heating	200 °C		6.3	8.5	19.5
	hydration state	-	-	0W/1W	1W	2W
ben_P	static heating	105 °C	W_{gt} [%]	8.0	13.3	28.9
	dynamic heating	250 °C		15.6	17.0	30.4
	hydration state	-	-	1W/2W	1W/2W	2W

The water content determined by dynamic heating was higher than the water content determined by static heating at 105 °C. This implies an incomplete removal of adsorbed water by static heating for smectite-rich clays with the commonly applied reference method. The underestimation of static W_{gt} in comparison to dynamic W_{gt} was most severe at low r.h. and reached up to 7.6% of absolute difference for ben_P. This is most likely a result of the

279 higher binding energy of the water molecules on the smectites at low relative humidity.
280 Complete removal of the strongly bound water required higher temperatures and therefore
281 resulted in a more severe underestimation of W_{gt} at 11% r.h. by static heating.
282 Due to their different interlayer occupation, the smectites of the bentonites showed different
283 hydration states with varying relative humidity (Figure 2). At 93% r.h. the smectites of all
284 three bentonites showed an expansion equalling a predominantly 2W hydration state and
285 ben_Cal reached a transition state 2W/3W according to Table 2 and [53]. At 43% r.h. ben_Cal
286 and ben_P primarily showed a 1W/2W transition state, whereas the smectite of ben_Vol
287 exhibited an expansion corresponding to 1W state. This behaviour displays the different
288 hydration properties of the interlayer cations (Table 1). Similarly, at low r.h. (11%) ben_Cal
289 and ben_P still showed a 1W/2W transition state, since these two contain the highest amount
290 of divalent cations within the interlayer and the hydration enthalpy of the cations decreases in
291 the order Ca^{2+} (-1920 kJ/mol) > Mg^{2+} (-1650 kJ/mol) > Na^{+} (-405 kJ/mol) [57]. Ben_Vol, with a
292 dominance of monovalent cations showed a 0W/1W transition state at 11% r.h..

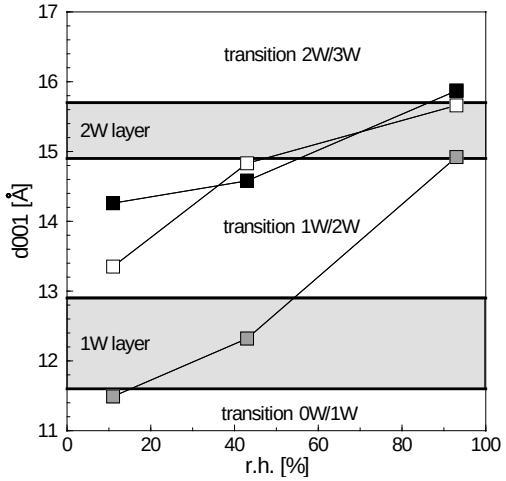

Figure 2: Basal spacing of the smectites in the bentonites in dependence of relative humidity.
ben_Cal (■),ben_Vol (▩), ben_P (□)

293

294 *Dielectric spectra*

295 The difference in hydration state and W_{gt} as a function of r.h. could furthermore be observed
296 in a changing dielectric behaviour. The real part of complex permittivity increases as a
297 function of water content over the whole frequency range (Figure 3).

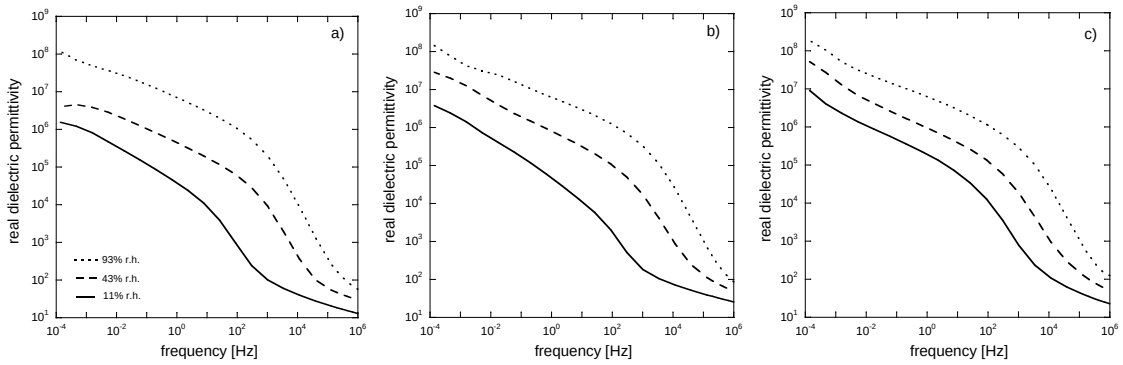

Figure 3: Real permittivity as a function of frequency for different r.h. a): ben_Cal, b): ben_Vol and c): ben_P; the legend on the left applies for all graphs.

298

299 The regions of steepest slope in the real permittivity plots are assumed to correspond to a
300 relaxation in the imaginary part of complex permittivity, although due to superimposing
301 conductivity effects, no clear relaxation peaks could be identified in the imaginary complex
302 permittivity. Thus, the three bentonite samples showed a relaxation shift to higher
303 frequencies with increasing moisture, which was more clearly seen in the dissipation factor
304 as discussed next.

305 For each of the bentonites, the dissipation factor was higher the higher the water content and
306 the peaks shifted to higher frequencies (Figure 4). The peaks in the range of 10^2 to 10^6 Hz
307 are assumed to be due to interfacial processes such as polarization in the electrochemical
308 double-layer at the clay/water interfaces. Hence, interfacial processes were promoted by an
309 increased water content.

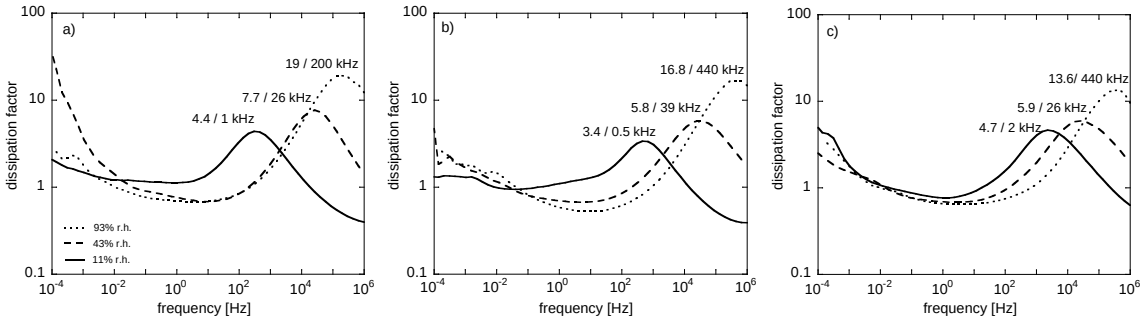

Figure 4: Dissipation factor as a function of frequency in dependence of water content; a): ben_Cal, b): ben_Vol and c): ben_P; the legend on the left applies for all graphs.

310

311 The increase of the dissipation factor to values >1 at the lower end of the frequency range,
312 showing where the dielectric losses outweigh the dispersion, is likely due to electrode
313 polarization.
314 Similarly to the plots of real permittivity, the moisture difference could clearly be observed in
315 the real conductivity plots (Figure 5). A conductivity plateau at upper frequencies of the
316 measurement range was visible for each sample at all of the studied relative humidities, from
317 which the ionic conductivity of the clays could be obtained (Table 5). Compared to ionic
318 conductivity measured in the clear supernatant of centrifuged bentonite suspensions, the
319 ionic conductivity of the samples stored at 93% r.h. is of about the same order of magnitude
320 (data not shown).
321

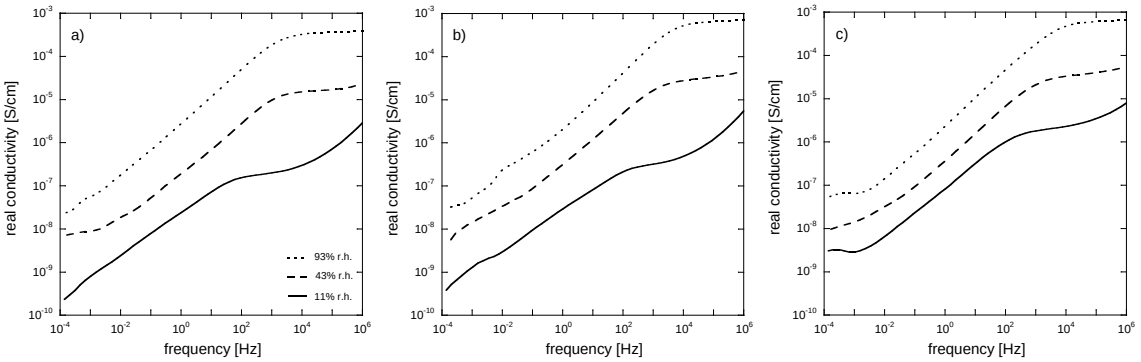

Figure 5: Real conductivity as a function of frequency for different r.h.; a): ben_Cal, b): ben_Vol and c): ben_P; the legend on the left applies for all graphs.
322

Table 5: Ionic conductivity of the bentonites obtained from the conductivity plateau in dependence of equilibrated moisture conditions.

sample	r.h. [%]	σ' [S/cm]
ben_Cal	11	1.5E-07
	43	1.3E-05
	93	3.0E-04
ben_Vol	11	1.8E-07
	43	2.4E-05
	93	5.7E-04
ben_P	11	1.7E-06
	43	2.9E-05
	93	5.2E-04

323

In all cases, the ionic conductivity of the bentonites increased with increasing water content, which is in agreement to the findings of Logsdon and Laird [58] and Bidadi *et al.* [59] who conducted dielectric studies of smectites at low water contents in the MHz range and on clay-films in the low frequency range, respectively.

Towards lower frequencies the conductivity plateau passed over to a linear section for each bentonite. The slope of the linear section was about 0.5, indicating diffusion at least as a participating underlying process in this frequency range.

Electrode polarization (EP) occurred at the lower end of the frequency range and was already indicated by the dissipation factor. The occurrence of EP was proven experimentally by measuring on bentonites with different sample thicknesses. The permittivity is a bulk quantity and should be independent of thickness, while the capacitance C~1/d, according to eq. (2). However, a spurious thickness dependence of the permittivity was observed at low frequencies, and this indicates the dominance of electrode polarisation at frequencies below 1 Hz. Thus, the behavior at the lower end of the frequency range can be assumed to be due to both bulk response and electrode polarization, whereas the higher end of the frequency range can be assumed to be mostly due to bulk response (Figure 6).

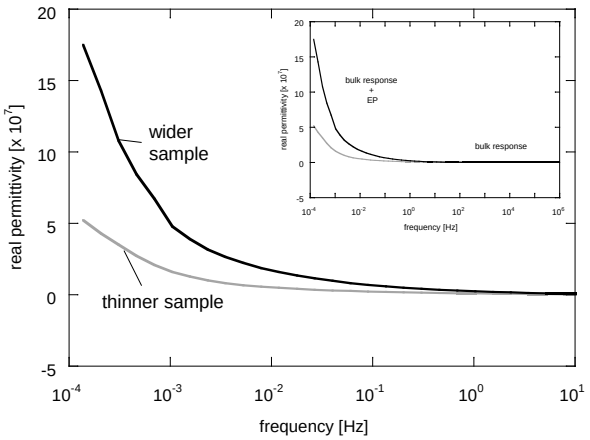

Figure 6: Real permittivity of ben_P at 43% r.h. and different sample thicknesses to identify electrode polarization; black curves: higher sample thickness (1.53 mm); grey curves: smaller sample thickness (0.97 mm).

Equivalent circuit modelling

Equivalent circuit modelling was frequently used in the past to identify the mechanisms taking place in clay suspensions and clay-water electrolyte systems, including smectitic clays, at low frequencies [40, 48]. Although some models were adjusted to describe double-layer polarization and Maxwell-Wagner polarization, and accounted for the accumulation of charges on the electrode due to electrode polarization, they showed to be completely inappropriate for the three presently studied bentonites at low moisture level. Hence, different dielectric mechanisms take place in clays dominated by free water rather than bound water and new equivalent circuit models are necessary to describe the effects taking place.

The following equivalent circuit model was chosen to describe the measured impedance and it is based on considerations of the physics of relaxation processes in a humid porous material. (Figure 7). The circuit contains constant phase elements (CPE) and resistances to account for bulk conductivity and electrochemical double-layer polarization.

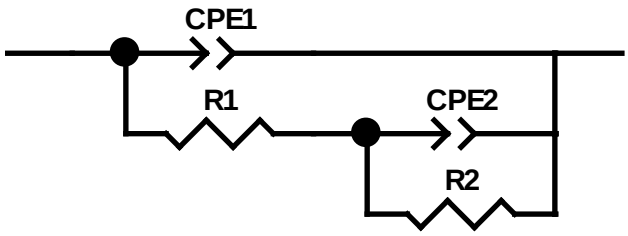

Figure 7: Equivalent circuit model representing the clay-water-mixture, consisting of resistances R1 and R2 and constant phase elements CPE1 and CPE2.

The CPEs were used instead of capacitors to account for heterogeneities in the relaxation at the clay-water-interface. The CPE impedance (Z_{CPE}) is characterized by the parameters *T* and *P* (eq. (8));

$$Z_{CPE} = \frac{1}{T(i\omega)^P}\,, \tag{8}$$

where $T = (\tau^{*P})/B$, *B* is the amplitude of Z_{CPE}, τ^* is a characteristic time constant and *P* an exponent varying between zero and one that describes the constant phase angle in the complex plane plot. A 45° line, signifying a diffusion process, is produced in the complex plane with *P* = 0.5. For *P* = 1, the CPE impedance equals that of a capacitor and for *P* = 0 that of a resistance.

The element CPE1 is attributed to the capacitive part of a high frequency relaxation, which can be due to bound water or to the Maxwell-Wagner effect [60]. Putting an additional resistance in series with CPE1 to model a high frequency relaxation did not improve the fit, and resulted in very high statistical errors in the value of the added series resistance. The resistance R1 is associated to the movement of ions dissolved in the adsorbed water in the pores of the bentonites. In addition, the series connection of R1 and CPE2 can be interpreted as a model of the electrochemical double-layer relaxation in the pore fluid close to the interfaces. Charges at the surface of the solid attract counter-ions of opposite charge and these give rise to the Stern layer. At a larger distance from the interface a diffuse layer develops at sufficiently high water content. The counter-ion concentration decreases with distance from the interface and the concentration of the oppositely charged ions increase. The double-layer relaxation of a sphere in a fluid has been studied frequently and a review of a number of approaches can be found in Nettelblad and Niklasson [61]. The most complete theory appears to be that of DeLacey and White [62]. It was found by Nettelblad and Niklasson [61] that a simple phenomenological expression of the Havriliak-Negami (HN [63]) type could give satisfactory fits to numerical results of the dielectric permittivity for a number of theories for the double-layer relaxation at a dielectric sphere. Hence we use the expression

$$C_{HN}(\omega) = \frac{A}{[1 + (i\omega\tau)^{1/2}]^2} \tag{9}$$

to represent the frequency-dependent capacitance of the double-layer relaxation. Here A is the relaxation strength and τ is the relaxation time. However, a porous material is not

composed of solid spheres, and in a porous structure the solid particles are connected to one another.

The dielectric response of a water-filled pore can be described by transmission line models [64]. The simplest model for a uniform pore assumes a distributed resistance along the pore and a distributed capacitance at the pore interface. A number of generalizations taking into account anomalous diffusion processes as well as trapping of charges were developed by Bisquert *et al.* [65, 66]. We then combined the transmission line approach with eq. (9) and took into account both the electrochemical double-layer relaxation and the conductivity due to ions dissolved in the pore fluid. The ion conduction process in the pore is represented by the resistances (R) in the upper part of Figure 8, while the double-layer relaxation is represented by the HN impedance connecting the resistance line with the pore interface.

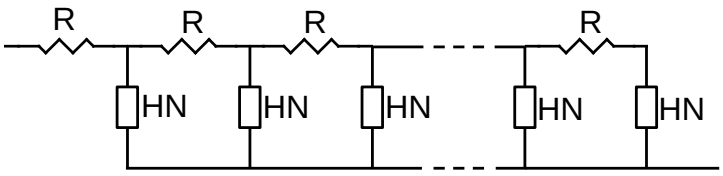

Figure 8: Transmission line for the double-layer relaxation in a single pore. The resistances describe ion conduction in the pore space, while HN is a Havriliak-Negami impedance representing the double-layer relaxation.

Converting the HN equation (eq. (9)) to impedance we find,

$$Z_{HN}(\omega) = \frac{\left[1+(i\omega\tau)^{1/2}\right]^2}{i\omega A}. \tag{10}$$

A transmission line has also a termination at the right hand end, which has not been specified in Figure 8. Considering the bulk part of the dielectric response and neglecting termination effects, gives the following impedance for the transmission line in Figure 8:

$$Z(\omega) = \left(R \cdot Z_{HN}(\omega)\right)^{1/2} = \frac{R^{1/2}\left(1+(i\omega\tau)^{1/2}\right)}{(i\omega A)^{1/2}}. \tag{11}$$

409 It is easily found that a series R-CPE circuit has an impedance

$$Z(\omega) = \frac{B+R(i\omega\tau^*)^P}{(i\omega\tau^*)^P}\ , \qquad (12)$$

410

411 which is found to be of the same form as equation (11) when the power-law exponent P = 0.5
412 The power law exponent of the double-layer relaxation may depart from the value 0.5 for a
413 variety of reasons, such as branched transmission line networks [67] or rough and fractal pore
414 surfaces [68]. We conclude that the occurrence of a series R-CPE combination in an
415 equivalent circuit analysis of experimental data can be interpreted in terms of a double-layer
416 relaxation. The interpretation of the series resistance R2 is more uncertain but we presume
417 that it is related to the termination of the transmission line. This resistance is important only
418 at the low frequency end of the spectra at < 1 Hz.

419

420 The fit parameters of the circuit described in Figure 7 are listed in Table 6. The model gives a
421 satisfactory description of the measured values (Figure 9) with low error estimates and sum
422 of X^2 ranging between 0.23 and 0.75 for all three bentonites.

423

Table 6: Fit parameters of the equivalent circuit model accounting for bulk effects and interfacial effects in clays at low moisture level. The fit parameters are given as resistivities/permittivities and are thus independent of sample geometry.

	r.h. [%]	sum X^2	CPE1-T [F/m*s$^{(1-P)}$]	CPE1-P	R1 [ohm*m]	CPE2-T [F/m*s$^{(1-P)}$]	CPE2-P	R2 [ohm*m]
ben_Cal	11	0.53	6.89E-10	0.74	487740	1.30E-07	0.55	8.72E+08
	43	0.51	4.82E-10	0.82	6801	7.51E-07	0.63	1.40E+07
	93	0.50	4.10E-08	0.56	273	1.29E-05	0.65	5.19E+06
ben_Vol	11	0.23	6.89E-10	0.78	269260	1.65E-07	0.50	1.49E+09
	43	0.75	2.59E-10	0.89	4066	1.36E-06	0.58	5.58E+07
	93	0.65	7.14E-07	0.43	133	1.22E-05	0.66	3.95E+06
ben_P	11	0.24	8.30E-09	0.64	34678	5.93E-07	0.61	3.27E+07
	43	0.29	1.12E-08	0.66	2941	1.93E-06	0.61	1.72E+07
	93	0.33	8.33E-08	0.57	180	9.90E-06	0.65	2.80E+06

424

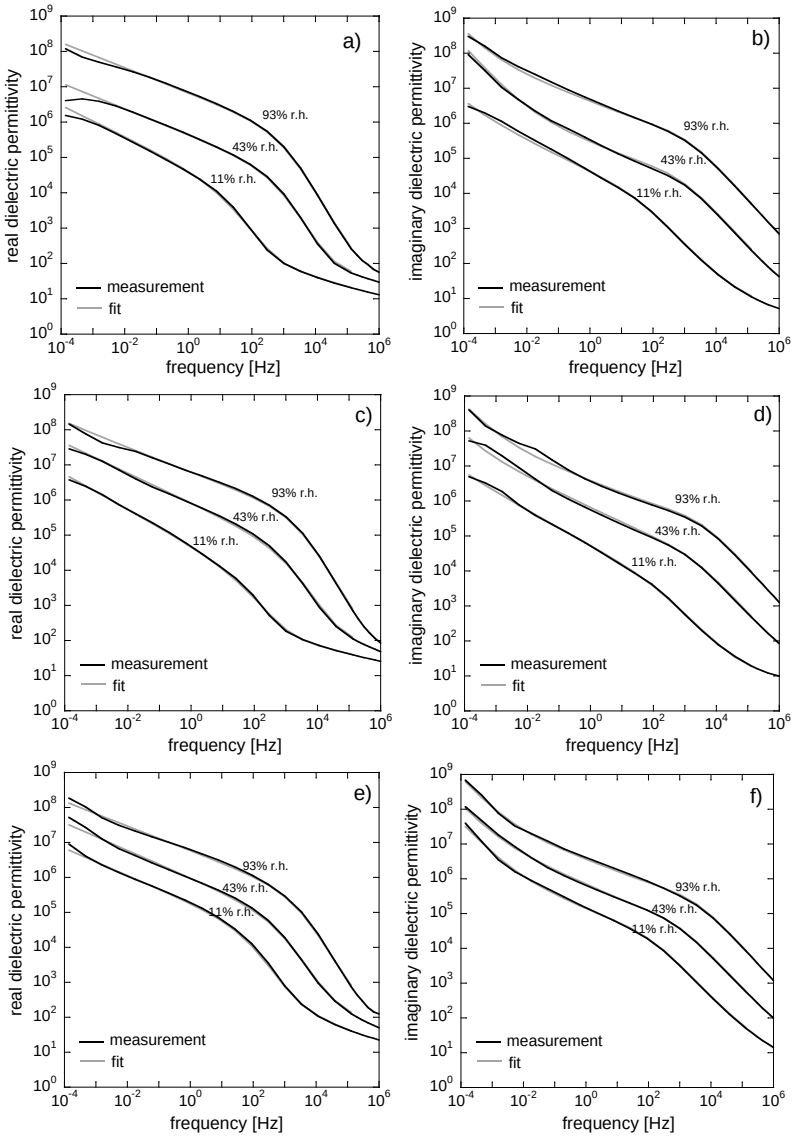

Figure 9: Fit results of the equivalent circuit described in Figure 7 at different r.h. conditions for ben_Cal (a, b), ben_Vol (c, d) and ben_P (e, f).

425

426 A relationship between W_{gt} as well as r.h. for each discrete circuit element was observed
427 (Figure 10). The resistivity of both elements R1 and R2 decreased with increasing moisture,
428 which is due to a better conductivity of the samples at higher water content (Table 5). At 11%
429 and 43% r.h. the resistivity of R1 decreased in the order ben_Cal < ben_Vol < ben_P
430 corresponding to the order of an increasing smectite content and increasing CEC. Hence, at
431 low water contents between 6 and 17% STA W_{gt}, a high amount of swellable 2:1 layer
432 silicates and a high ability to reversibly exchange cations resulted in a reduced bulk
433 resistivity. This implies that the Cu-Trien exchangeable cations, preferably those bound to
434 the smectitic surface, are responsible for the conductivity at least at water contents up to

17% W_{gt}. At those low water contents the interlayer cations are possibly as strongly bound as the cations associated with the outer clay mineral surface forming the Stern layer.

At water contents of 19% STA W_{gt} and above other parameters than smectite content and CEC seemed to become more important. At 93% r.h. the resistivity of R1 increases in the order benVol < benP < benCal which corresponds to the order of the basal spacing d*001* and to the amount of divalent cations within the interlayer (Table 1 and Table 2).

This coincides with findings in the literature [10, 69] with slightly different thresholds. Herein it was concluded that the reorientation of water molecules bound to clays with a water content of up to 4% W_{gt} takes significantly longer than the reorientation of water molecules bound to clays with water contents of about 13% $W_{gt.}$ Hereby, a longer reorientation time of bound water molecules was assumed to be associated with a stronger binding of the water molecules to the interlayer cation of the clay mineral. Further, the reorientation of the water molecules bound to the interlayer cation showed to be different from that of remaining water [10, 70]. However, further analysis, for instance with homoionically exchanged samples, are necessary to clearly attribute the behavior to individual processes.

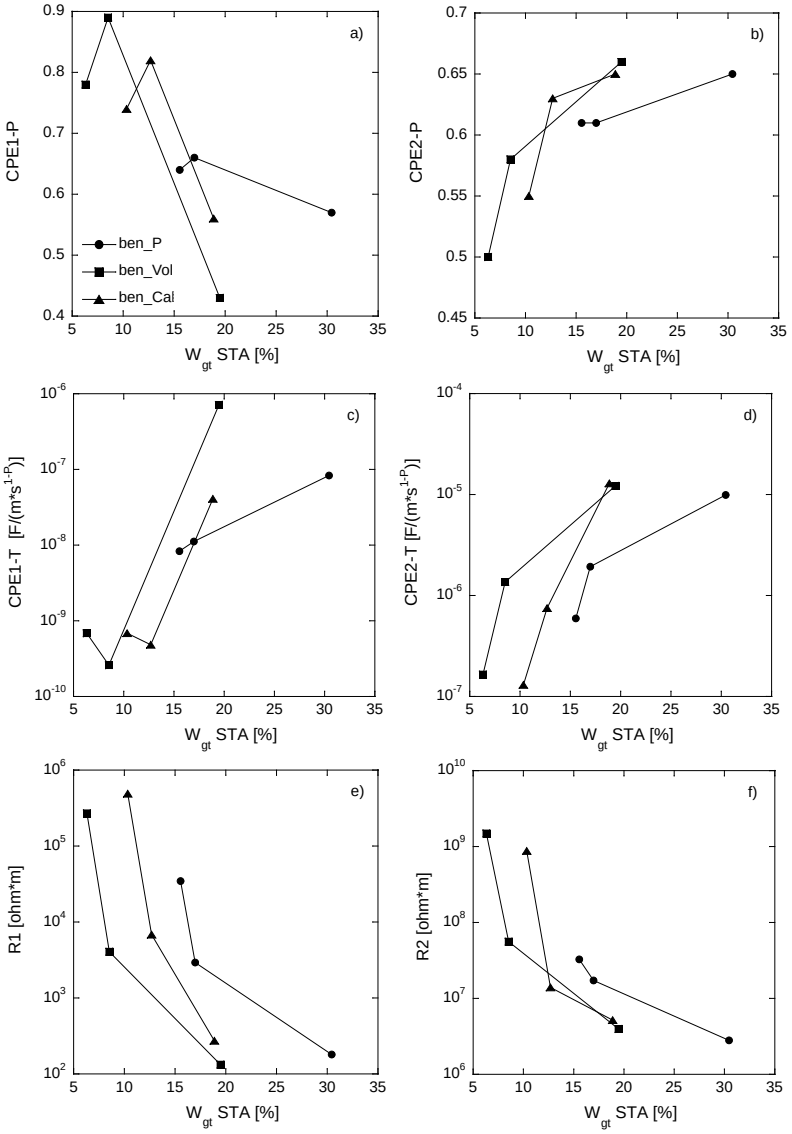

Figure 10: Relationship of discrete circuit elements and STA W_{gt} for the equivalent circuit model of Figure 7**;** the legend in plot a) applies for all graphs.

451

452 The corresponding capacitive element CPE1 of the bulk response showed a similar behavior
453 of ben_Vol and ben_Cal, whereas ben_P seemed to be characterized by partly different
454 processes (Figure 10).

455 The exponent *P* of CPE1, describing the constant phase angle in the complex plane plot,
456 was always highest at intermediate relative humidities and increased in the order
457 93% r.h. < 11% r.h. < 43% r.h. (Table 6, Figure 10). At 93% r.h. the CPE1 *P* values ranged
458 between 0.43 and 0.56 and at 43% r.h. between 0.66 and 0.89. For ben_P the constant
459 phase angle showed little variation (0.57 … 0.66) between the studied moisture states. A *P*
460 value of about 0.5 suggests diffusion as a contributing mechanism. At very low relative

humidities the *CPE2 P* values that characterize the interfacial double-layer relaxation process, suggest a possible occurrence of diffusion for the two bentonites ben_Cal and ben_Vol (0.55 and 0.5, respectively). With increasing relative humidity the exponent departs more and more from the value 0.5 .

The occurrence of electrode polarization was proven for ben_P (Figure 6) and is also likely to be present in ben_Vol and ben_Cal at low frequencies. In order to assess the thickness dependency of the discrete circuit elements, the model of Figure 7 was applied to ben_P at 43% r.h. for different sample thicknesses (1.53 mm vs. 0.97 mm). Equivalent circuit modeling on samples of different thickness was performed on impedance level, hence without correction for area and thickness of the sample. Hereby, the circuit element R1 was larger for the thicker sample, which supports the interpretation that it describes the bulk resistivity. In addition, CPE1-T was characterized by almost the same thickness dependency as R1, strongly indicating that these elements are coupled and represent a single mechanism. The other resistance R2 influenced the spectra below 0.1 Hz for ben_P at 43% r.h. It showed lower values for thicker samples, i.e. the opposite behavior to R1. This behavior is clearly not a bulk one and is presumed to be due to a termination of the transmission line or to charge transfer mechanisms at the electrodes.

In a second model (Figure 11) a separate capacitor was added in series with the other discrete circuit elements in order to separate a possible capacitive part of the electrode polarization effect from other processes. It led to better fits at intermediate and high water contents for ben_P, as seen in Table 7.

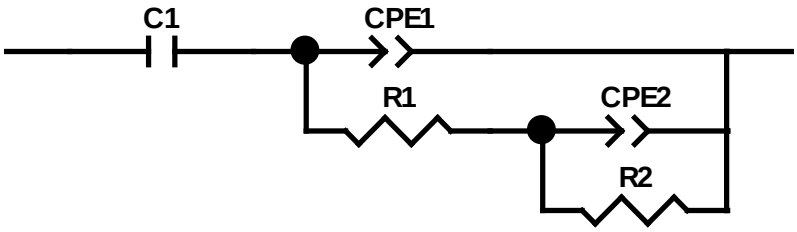

Figure 11: Equivalent circuit model for a bentonite of high purity (ben_P) that separately accounts for capacitive effects of electrode polarization.

Table 7: Fit parameters of ben_P for the model given in Figure 11.

r.h. [%]	sum X^2	C1 [F]	CPE1-T [$F/s^{(1-P)}$]	CPE1-P	R1 [ohm]	CPE2-T [$F/s^{(1-P)}$]	CPE2-P	R2 [ohm]
43	0.0797	0.0006	3.31E-07	0.44	3480	1.49E-06	0.65	1.38E+07
93	0.2894	0.0073	6.31E-08	0.60	181	9.72E-06	0.65	2.50E+06

The second model (Figure 11) depended on the smectite content of the bentonite and the water content. It worked reliably at intermediate and high relative humidities for high smectite contents. At 11% r.h. and for the two bentonites with a higher amount of impurities, the model was characterized by high errors and high sum of X^2 values.

The build-up of charges on the electrode was higher at higher water content, as could be described by the capacitor C1 (Table 7). The accumulated charges gave rise to capacitance values in the range of $0.6*10^{-3}$ and $7.3*10^{-3}$ F for ben_P.

Nevertheless, it can be expected that electrode polarization exists for the bentonites with lower smectite content and possibly for ben_P at 11% r.h.. However, then EP could not clearly be separated from the other processes in the equivalent circuit.

SUMMARY AND CONCLUSIONS

The low frequency dielectric properties of three bentonites with varying smectite content were analyzed after storage at defined relative humidity. The clays exhibited low water contents ranging between 6 and 30% STA W_{gt}.

Dielectric properties were clearly influenced by hydration state and water content. Real dielectric permittivity and real conductivity increased with increasing amount of adsorbed water. The imaginary dielectric permittivity showed no clear relaxation peak due to superimposing conductivity effects. However, the dissipation factor $tan\,\delta$ revealed clear peaks for each of the bentonites in the range of 10^2 to 10^6 Hz that were attributed to interfacial polarization such as polarization in the electrochemical double layer at the clay-water interface. The intensity of the interfacial processes were promoted by increased water content and shifted to higher frequencies.

The occurrence of electrode polarization was shown to be a participating process at the lower end of the frequency range (~ < 1 Hz). However, separating electrode polarization from other processes in equivalent circuit modeling could only be achieved for the purest of the bentonites (ben_P) with a smectite content of 98%. The charges that accumulated on the electrode gave rise to capacitance values of about $0.6*10^{-3}$ and $7.3*10^{-3}$ F.

An equivalent circuit model consisting of a combination of CPEs and resistances was found to successfully describe the low frequency dielectric behavior of bentonites at adsorbed water states. A series R-CPE connection was used to model the electrochemical double-layer relaxation in the pore fluid close to the interfaces. Equivalent circuit modelling further revealed that bulk resistivity was mainly influenced by the smectite content and CEC at water contents up to 17% STA W_{gt}. At water contents of ≥ 19% STA W_{gt} structural parameters of the interlayer, such as interlayer occupation and clay mineral swelling due to water uptake into the interlayer predominantly influenced the bulk resistivity.

In order to validate our model on a larger set of materials and ascertain the importance of different structural and mineralogical parameters on the dielectric response, further dielectric

526 analysis on clays at low moisture levels, especially homoionic exchanged bentonites, are
527 necessary and currently performed.
528
529 ACKNOWLEDGEMENTS
530 The measurements in the low frequency range were implemented at the Division of
531 Nanotechnology and Functional Materials at Uppsala University (UU) in Sweden. We like to
532 thank the Karlsruhe House of Young Scientists (KHYS) for financial support allowing a
533 research exchange to UU. We are furthermore grateful to Süd-Chemie AG for providing the
534 studied materials, Dr. Ken Welch for support during the measurements and Marita Heinle for
535 performing ICP-OES measurements.
536
537

REFERENCES

[1] Velde, B.; Meunier, A., *The origin of clay minerals in soils and weathered rocks*, Springer: Heidelberg, (2008).
[2] Wolters, F.; Lagaly, G.; Kahr, G.; Nueesch, R.; Emmerich, K., *Clays and Clay Minerals*, (2009) **57**, 115.
[3] Laird, D. A., *Applied Clay Science*, (2006) **34**, 74.
[4] Dontsova, K. M.; Norton, L. D.; Johnston, C. T.; Bigham, J. M., *Soil Sci Soc Am J*, (2004) **68**, 1218.
[5] Emmerich, K.; Wolters, F.; Kahr, G.; Lagaly, G., *Clays and Clay Minerals*, (2009) **57**, 104.
[6] Costanzo, P. M., *Clays and Clay Minerals*, (2001) **49**, 372.
[7] Mihranyan, A.; Ferraz, N.; Strømme, M., *Progress in Materials Science*, (2012) **57**, 875.
[8] Cases, J. M.; Berend, I.; Francois, M.; Uriot, J. P.; Michot, L. J.; Thomas, F., *Clays and Clay Minerals*, (1997) **45**, 8.
[9] Bérend, I.; Cases, J.-M.; Francois, M.; Uriot, J.-P.; Michot, L.; Masion, A.; Thomas, F., *Clays and Clay Minerals*, (1995) **43**, 324.
[10] Sposito, G.; Prost, R., *Chemical Reviews*, (1982) **82**, 553.
[11] Fripiat, J. J.; Stone, W. E. E., *Physics and Chemistry of Liquids*, (1978) **7**, 349
[12] Young, D. A.; Smith, D. E., *The Journal of Physical Chemistry B*, (2000) **104**, 9163.
[13] Ferrage, E.; Lanson, B.; Sakharov, B. A.; Drits, V. A., *American Mineralogist*, (2005) **90**, 1358.
[14] Behari, J., *Microwave dielectric behavior of wet soils*, van der Meer, F. D. Ed. Springer: New York, (2005).
[15] Robinson, D. A.; Jones, S. B.; Wraith, J. M.; Or, D.; Friedman, S. P., *Vadose Zone J*, (2003) **2**, 444.
[16] Kaatze, U.; Hübner, C., *Measurement Science and Technology*, (2010) **21**, 082001.
[17] Baghadadi, N.; Holah, N.; Zribi, M., *International Journal of Remote Sensing*, (2006) **27**, 1907.
[18] Kanoun, O.; Tetyuev, A.; Tränkler, H.-R., *Technisches Messen*, (2004) **71**, 475.
[19] Kirda, C.; Reichhardt, K., Measurement problems associated with soil water studies using nuclear techniques, In *Potential of forage legumes in farming systems in Sub-Saharan Africa*, Hague, I.; Jutzi, S.; Neate, P. J. H. Eds.; Ilca, Ethiopia, (1985).
[20] Gelin, K.; Bodin, A.; Gatenholm, P.; Mihranyan, A.; Edwards, K.; Strømme, M., *Polymer*, (2007) **48**, 7623.
[21] Jönsson, M.; Welch, K.; Hamp, S.; Strømme, M., *The Journal of Physical Chemistry B*, (2006) **110**, 10165.
[22] Brohede, U.; Bramer, T.; Edsman, K.; Strømme, M., *The Journal of Physical Chemistry B*, (2005) **109**, 15250.
[23] Nilsson, M.; Strømme, M., *The Journal of Physical Chemistry B*, (2005) **109**, 5450.
[24] Bell, J. P., *IH Report No. 19*, (1987), 51.
[25] Kaden, H.; Königer, F.; Schuhmann, R.; Niklasson, G.; Emmerich, K., Detection of moisture differences of a swellable and a non-swellable clay in the low and mid frequency range, In *6th Conference on Innovative Moisture Measurement in Research and Practice*, Karlsruhe, Germany, (2011); pp 157.
[26] Hallikainen, M. T.; Ulaby, F. T.; Dobson, M. C.; El-Rayes, M. A.; Wu, L.-K., *Geoscience and Remote Sensing, IEEE Transactions on*, (1985) **GE-23**, 25.
[27] Perdok, U. D.; Kroesbergen, B.; Hilhorst, M. A., *European Journal of Soil Science*, (1996) **47**, 367.
[28] Scholte, J.; Shang, J.; Rowe, R., *Geotechnical Testing Journal*, (2001),
[29] Shang, J.; Rowe, R.; Umana, J.; Scholte, J., *Geotechnical Testing Journal*, (1998) **22**,
[30] Birchak, J. R.; Gardner, C. G.; Hipp, J. E.; Victor, J. M., *Proceedings of the IEEE*, (1974) **62**, 93.
[31] Bridge, B.; Sabburg, J.; Habash, K.; Ball, J.; Hancock, N., *Australian Journal of Soil Research*, (1996) **34**, 825.

[32] Robinson, D. A.; Bell, J. P.; Batchelor, C. H., *Journal of Hydrology*, (1994) **161**, 169.
[33] Kaviratna, P. D.; Pinnavaia, T. J.; Schroeder, P. A., *Journal of Physics and Chemistry of Solids*, (1996) **57**, 1897.
[34] Roy, G.; Pelletier, M.; Thomas, F.; Despas, C.; Bessiere, J., *Clay Minerals*, (2000) **35**, 335.
[35] Hall, P. G.; Rose, M. A., *J. Chem. Soc., Faraday Trans.*, (1978) **74**, 1221.
[36] Lockhart, N. C., *Journal of Colloid and Interface Science*, (1980) **74**, 509.
[37] Lockhart, N. C., *Journal of Colloid and Interface Science*, (1980) **74**, 520.
[38] Raythatha, R.; Sen, P. N., *Journal of Colloid and Interface Science*, (1986) **109**, 301.
[39] Blum, G.; Maier, H.; Sauer, F.; Schwan, H. P., *The Journal of Physical Chemistry*, (1995) **99**, 780.
[40] Dudley, L. M.; Bialkowski, S.; Or, D.; Junkermeier, C., *Soil Sci Soc Am J*, (2003) **67**, 518.
[41] Ishida, T.; Kawase, M.; Yagi, K.; Yamakawa, J.; Fukada, K., *Journal of Colloid and Interface Science*, (2003) **268**, 121.
[42] Shang, J. Q.; Lo, K. Y.; Inculet, I. I., *Journal of Geotechnical Engineering*, (1995) **121**, 243.
[43] Carrier, M.; Soga, K., *Engineering Geology*, (1999) **53**, 115.
[44] Wübbenhorst, M.; Van Turnhout, J., *Dielectric Newsletter NOVOCONTROL*, (2000) **14**,
[45] Wübbenhorst, M.; van Turnhout, J., *Journal of Non-Crystalline Solids*, (2002) **305**, 40.
[46] Schwan, H. P., *Radiation and Environmental Biophysics*, (1966) **3**, 181.
[47] Kremer, F.; Schönhals, A., *Broadband dielectric Spectroscopy*, Springer: Heidelberg, (2003).
[48] Klein, K.; Santamarina, J. C., *Journal of Geotechnical Engineering*, (1996) **122**, 954.
[49] Meier, L. P.; Kahr, G., *Clays and Clay Minerals*, (1999) **47**, 186.
[50] Brunauer, S.; Emmett, P. H.; Teller, E., *Journal of the American Chemical Society*, (1938) **60**, 309.
[51] Sing, K., *Colloids and Surfaces A: Physicochemical and Engineering Aspects*, (2001) **187-188**, 3.
[52] Kaden, H.; Königer, F.; Schuhmann, R.; Emmerich, K., Water adsorption hysteresis of swellable and non-swellable clays and soils detected with dielectric spectroscopy and thermal analysis, In *1st European Conference on Moisture Measurement*, Kupfer, K. Ed. Weimar, Germany, (2010); pp 238.
[53] Ferrage, E.; Lanson, B.; Michot, L. J.; Robert, J.-L., *The Journal of Physical Chemistry C*, (2010) **114**, 4515.
[54] Michot, L. J.; Ferrage, E.; Jiménez-Ruiz, M.; Boehm, M.; Delville, A., *The Journal of Physical Chemistry C*, (2012) **116**, 16619.
[55] DIN18121-1, Baugrund, Untersuchung von Bodenproben - Wassergehalt, Teil 1: Bestimmung durch Ofentrocknung, In Deutsches Institut für Normung e.V.: (1998).
[56] Gråsjö, J.; Welch, K.; Strømme, M., *Applied Physics Letters*, (2008) **93**, 092901.
[57] Atkins, P. W., *Physikalische Chemie*, Wiley: Weinheim, (2002).
[58] Logsdon, S. D.; Laird, D. A., *Clays and Clay Minerals*, (2004) **52**, 411.
[59] Bidadi, H.; Schroeder, P. A.; Pinnavaia, T. J., *Journal of Physics and Chemistry of Solids*, (1988) **49**, 1435.
[60] Leroy, P.; Revil, A., *J. Geophys. Res.*, (2009) **114**, B10202.
[61] Nettelblad, B.; Niklasson, G. A., *Journal of Colloid and Interface Science*, (1996) **181**, 165.
[62] DeLacey, E. H. B.; White, L. R., *Journal of the Chemical Society, Faraday Transactions 2: Molecular and Chemical Physics*, (1981) **77**, 2007.
[63] Havriliak, S.; Negami, S., *Journal of Polymer Science Part C: Polymer Symposia*, (1966) **14**, 99.
[64] Raistrick, I. D., *Electrochimica Acta*, (1990) **35**, 1579.
[65] Bisquert, J.; Compte, A., *Journal of Electroanalytical Chemistry*, (2001) **499**, 112.
[66] Bisquert, J.; Vikhrenko, V. S., *Electrochimica Acta*, (2002) **47**, 3977.
[67] Scheider, W., *The Journal of Physical Chemistry*, (1975) **79**, 127.

649 [68] Bisquert, J.; Garcia-Belmonte, G.; Fabregat-Santiago, F.; Bueno, P. R., *Journal of*
650 *Electroanalytical Chemistry*, (1999) **475**, 152.
651 [69] Calvet, R., Absoption dipolaire et conductivite de l'eau adsorbee sur la
652 montmorillonite calcique, In *Proc. Int. Clay Conf*, (1972).
653 [70] Cebula, D. J.; Thomas, R. K.; White, J. W., *Clays and Clay Minerals*, (1981) **29**, 241.

654

655